Supplementary material for Investigation of stochastic-threshold incision models across a climatic and morphological gradient

Desormeaux C., Godard V., Lague D., Duclaux G.
Fleury J., Benedetti L., Bellier O., ASTER Team

October 26, 2021

1 Cosmogenic nuclides

1.1 ^{10}Be concentration measurements

Measuring cosmogenic nuclides concentrations in river sands is now a standard approach in geomorphology allowing to determine the rates of denudation processes at the scale of landscapes [von Blanckenburg, 2005]. Bulk sand samples were sieved to extract the 250-1000 μm fraction, which was then submitted to magnetic separation. The remaining fraction was leached with 37% HCl to remove carbonate fragments. The samples were then repetitively leached with H_2SiF_6 and submitted to mechanical shaking until pure quartz was obtained. Removal of atmospheric ^{10}Be from grain surfaces was achieved by a series of three successive leachings in concentrated HF, each leaching removing 10% of the sample mass [Brown et al., 1991]. After addition of an in-house ^{9}Be carrier ($\sim$150 μl at 3.03 x 10^{-3} g/g [Merchel et al., 2008]), the samples were digested in concentrated HF and Be was isolated for measurements using ion-exchange chromatography. ^{10}Be measurements were performed by the ASTER Team at the French AMS National Facility, located at CEREGE in Aix-en-Provence. ^{10}Be/^{9}Be ratios were calibrated against the STD-11 standard by using an assigned value of $1.191 \pm 0.013 \times 10^{-11}$ [Braucher et al., 2015].

Uncertainties on ^{10}Be concentrations (reported as 1σ) are calculated according to the standard error propagation method using the quadratic sum of the relative errors and include a conservative 0.5% external machine uncertainty [Arnold et al., 2010], a 1.08% uncertainty on the certified standard ratio, a 1σ uncertainty associated to the mean of the standard ratio measurements during the measurement cycles, a 1σ statistical error on counted ^{10}Be events and the uncertainty associated with the chemical and analytical blank correction. We processed 5 blanks along with our samples, with characteristics reported in table S2.

1.2 Denudation rates calculations

We computed steady-state denudation rates (table S1), with the online calculator described in Balco et al. [2008] and the nuclide specific LSD scaling scheme of Lifton et al. [2014], using the CRONUS-Earth calibration dataset [Borchers et al., 2016] for the calculation of spallation production rates and muon production rates according to Balco [2017]. We used 160 g/cm^2 for the effective neutron attenuation length in rock, and a global density of 2.65 g/cm^3. No shielding correction was considered [DiBiase, 2018].

Table S1: Cosmogenic nuclides data : ^{10}Be results

Sample	Latitude (°)	Longitude (°)	Mass[a] (g)	Be Carrier[b] (g)	$^{10}Be/^{9}Be$[c,d] ($x10^{-14}$)	$[^{10}Be]$[e] ($x10^3$ at/g)	^{10}Be denudation rate[e,f] (mm/ka)	Integration time scale[g] (ka)
CDX-01	44.1571	4.0228	20.80	0.1489	4.15±0.28	60.11±3.99	75.39±9.05	8
CDX-02	44.0371	3.8608	20.18	0.1567	3.85±0.28	60.38 ± 4.40	81.76 ± 10.12	7
CDX-03	44.1701	3.8398	19.81	0.1516	3.73±0.29	57.63±4.54	87.34 ± 11.12	7
CDX-04	44.1599	3.8078	20.27	0.1515	3.30±0.32	49.87 ± 4.79	104.30 ± 14.47	6
CDX-05	44.1268	3.7623	20.78	0.1517	3.21±0.29	47.42 ± 4.23	114.11 ± 15.29	5
CDX-06	44.1259	3.7610	19.31	0.1527	3.56±0.38	56.93 ± 6.11	90.13 ± 13.22	7
CDX-07	44.6702	4.1888	16.90	0.1528	4.10±0.31	74.87 ± 5.62	91.18 ± 11.40	7
CDX-08	44.9011	3.5527	20.28	0.1530	15.97±0.85	243.47 ± 12.93	32.95 ± 3.73	18
CDX-09	44.8228	3.6144	20.82	0.1518	23.45±1.08	345.53 ± 15.96	24.34 ± 2.68	25
CDX-10	44.7662	3.6321	18.02	0.1522	18.16±0.89	310.15 ± 15.18	27.20 ± 3.03	22
CDX-11	44.6491	3.8964	20.86	0.1526	13.24±0.76	195.85 ± 11.23	39.23 ± 4.53	15
CDX-12	44.6479	3.9028	20.56	0.1529	12.28±0.70	184.67 ± 10.56	41.80 ± 4.82	15
CDX-13	44.5107	3.4113	19.60	0.1515	10.46±0.42	163.46 ± 6.51	40.10 ± 4.32	15
CDX-14	44.2809	3.6963	18.42	0.1532	3.08±0.21	51.73 ± 3.59	126.15 ± 15.36	5
CDX-15	44.2444	3.9254	20.29	0.1476	2.97±0.29	43.72 ± 4.21	117.30 ± 16.28	5
CDX-16	44.8133	4.5919	19.23	0.1558	4.95±0.33	80.99 ± 5.39	66.69 ± 8.01	9
CDX-17	44.8253	4.4961	20.20	0.1548	5.49±0.38	84.98 ± 5.86	73.62 ± 8.94	8
CDX-18	44.8769	4.5324	18.36	0.1551	6.64±0.36	113.45 ± 6.09	51.20 ± 5.81	12
CDX-19	44.9006	4.4154	17.60	0.1550	3.65±0.32	65.03 ± 5.71	95.49 ± 12.70	6
CDX-20	44.9821	4.5683	15.22	0.1552	6.34±0.33	130.62 ± 6.87	41.36 ± 4.67	15
CDX-21	45.1184	4.2875	17.93	0.1552	10.05±0.72	175.96 ± 12.53	38.94 ± 4.78	15
CDX-22	45.1401	4.2937	20.33	0.1551	14.01±0.78	216.11 ± 11.97	31.40 ± 3.59	19
CDX-23	45.2098	4.3806	19.67	0.1547	12.06±0.89	191.79 ± 14.09	37.08 ± 4.60	16
CDX-24	45.1622	4.7134	19.76	0.1548	10.66±0.50	168.73 ± 7.84	32.49 ± 3.58	19
CDX-25	45.0736	4.6621	19.60	0.1544	9.79±0.53	155.77 ± 8.40	35.21 ± 4.00	17
CDX-26	45.0598	4.4951	14.52	0.1553	6.61±0.68	143.00 ± 14.62	46.26 ± 6.62	13
CDX-27	45.0591	4.4943	19.52	0.1556	6.86 ± 0.34	110.44 ± 5.46	58.99 ± 6.58	10
CDX-28	44.9697	3.4103	18.13	0.1543	16.26 ± 0.90	279.70 ± 15.46	29.08 ± 3.32	21
CDX-29	45.0810	3.3130	16.52	0.1466	12.04 ± 1.10	215.88 ± 19.67	33.53 ± 4.54	18
CDX-30	44.9735	3.2168	20.41	0.1550	10.81 ± 0.40	165.88 ± 6.13	37.19 ± 3.97	16
CDX-31	44.8773	2.9991	20.85	0.1540	10.57 ± 0.89	157.78 ± 13.21	42.40 ± 5.53	15
CDX-32	44.8249	3.1096	20.11	0.1547	13.31 ± 1.07	207.03 ± 16.71	35.80 ± 4.60	17
CDX-33	44.8256	3.3706	20.11	0.1546	15.62 ± 0.83	242.69 ± 12.95	31.35 ± 3.55	19
CDX-34	44.7086	3.3834	21.00	0.1539	12.95 ± 1.02	191.74 ± 15.10	41.87 ± 5.33	14

[a] Dissolved pure quartz mass. [b] Be in-house carrier mass, ∼150 μl at 3.03 x 10^{-3} g/g [Merchel et al., 2008]. [c] $^{10}Be/^{9}Be$ ratios were calibrated against the STD-11 standard by using an assigned value of $1.191 \pm 0.013 \times 10^{-11}$ [Braucher et al., 2015]. [d] See text for details on the uncertainties on AMS measurements. [e] Uncertainties are reported at the 1σ level. [f] See text for details on the calculation procedure for denudation rates. [g] Averaging timescales according to von Blanckenburg [2005].

Table S2: Cosmogenic nuclides data :Process blanks

Sample	Be Carrier[a] (g)	$^{10}Be/^{9}Be$[b] ($x10^{-16}$)	$+1\sigma$ ^{10}Be atoms[c] ($x10^{3}$)	Average ratio[d]	Min ratio[e]
CDX-bl1	0.1565	8.02±1.85	31.21	40±4	34
CDX-bl2	0.1517	18.85±3.96	69.95	58±32	14
CDX-bl3	0.1575	10.10±2.18	41.89	58±28	30
CDX-bl4	0.157	9.45±2.37	37.50	94±29	60
CDX-bl5	0.1572	9.91±2.41	39.13	100±22	62

[a] Be in-house carrier mass, ∼150 μl at 3.025 x 10^{-3} g/g [Merchel et al., 2008]. [b] $^{10}Be/^{9}Be$ ratios were calibrated against the STD-11 standard by using an assigned value of $1.191 \pm 0.013 \times 10^{-11}$ [Braucher et al., 2015].
[c] Calculated with the upper 1σ bound on $^{10}Be/^{9}Be$ ratio. [d] For each blank : mean and standard deviation of the ratios between the number of ^{10}Be atoms in the samples (processed with the blank) and the $+1\sigma$ bound on ^{10}Be atoms in the blank. [e] For each blank : minimum value of ratios between the number of ^{10}Be atoms in the samples (processed with the blank) and the $+1\sigma$ bound on ^{10}Be atoms in the blank.

2 Hydrological and morphometric analysis

Here we report the supplementary figures and tables related to the hydrological and morphometric analysis.

Table S3: Basins parameters

Basin ID	Regional setting [a]	Area[b] (km^2)	Mean elevation [b] (m)	Relief [b] (m)	Slope[b] (°)	Precipitation[c] (mm/a)	Runoff[g] (mm/a)	k[h]	Concavity[i]	k_{sn} $m^{0.9}$ [j]	Lithology[k]
CDX-01	RH-C	73	478	763	20.18	1452	942	0.42	0.57	35	Schist
CDX-02	RH-C	39	588	907	19.59	1516	1012	0.34	0.75	54	Schist
CDX-03	RH-C	84	609	901	21.55	1529	1026	0.51	0.8	51	Schist
CDX-04	RH-C	92	651	843	21.03	1441	930	0.53	0.87	66	Schist
CDX-05	RH-C	66	705	886	24.05	1498	992	0.5	0.73	47	Schist
CDX-06	RH-C	31	641	738	25.18	1505	1000	0.43	0.59	33	Schist
CDX-07	RH-A	74	992	1105	24.3	1820	1342	0.65	0.65	97	Orthogneiss
CDX-08	LO	44	1230	398	6.8	933	378	1.98	0.56	33	Granite
CDX-09	LO	54	1297	373	6.78	886	327	1.78	0.81	29	Granite
CDX-10	LO	47	1303	345	6.27	882	322	1.57	0.27	22	Granite
CDX-11	LO	77	1175	528	13.31	1208	677	0.84	0.66	24	Orthogneiss
CDX-12	LO	47	1179	518	14.1	1348	829	0.74	0.58	23	Orthogneiss
CDX-13	GR	34	958	591	15.2	1030	483	1.51	0.77	57	Paragneiss
CDX-14	GR	75	957	734	17.97	1470	962	0.64	0.59	33	Schist
CDX-15	RH-C	85	634	1058	21.95	1590	1092	0.56	0.73	46	Schist
CDX-16	RH-A	59	692	1115	20.77	1186	653	0.58	0.51	63	Granite
CDX-17	RH-A	43	887	883	19.43	1311	789	0.6	0.51	65	Granite
CDX-18	RH-A	43	789	880	19.5	1207	676	0.62	0.42	58	Granite
CDX-19	RH-A	75	875	982	20.18	1343	823	0.68	0.52	59	Granite
CDX-20	RH-A	37	694	808	16.51	1098	557	0.7	0.62	57	Orthogneiss
CDX-21	LO	49	1013	380	7.26	1078	535	1.23	0.24	30	Orthogneiss
CDX-22	LO	21	1000	339	5.5	1065	521	1.35	0.46	26	Orthogneiss
CDX-23	LO	67	1060	592	11.44	1059	515	1.39	0.53	40	Orthogneiss
CDX-24	RH-A	95	706	957	15.81	995	445	1.12	0.48	53	Orthogneiss
CDX-25	RH-A	62	712	795	16.52	1040	494	0.93	0.47	49	Orthogneiss
CDX-26	RH-A	74	959	771	17.5	1102	561	1.11	0.43	58	Orthogneiss
CDX-27	RH-A	35	939	657	16.66	1151	615	1.02	0.61	71	Orthogneiss
CDX-28	LO	31	1248	482	9.44	943	389	2.04	0.29	42	Granite
CDX-29	LO	38	1085	533	9.01	855	293	1.87	0.28	39	Granite
CDX-30	GR	3.65	876	209	6.47	805	239	1.86	0.13	29	Orthogneiss
CDX-31	GR	53	983	625	9.8	1085	543	1.87	0.18	53	Granite
CDX-32	GR	61	1124	358	6.39	1029	482	1.78	0.35	33	Granite
CDX-33	GR	32	1154	573	7.92	949	395	1.95	0.46	59	Granite
CDX-34	GR	41	1231	509	7.62	911	354	1.76	0.41	45	Granite

[a] Studied areas. RH-C: Rhône-Cévennes, RH-A: Rhône-Ardèche, LO: Loire upper catchment and GR: Garonne upper catchment. [b] Calculated from 25 m resolution Digital Elevation Model (IGN BD ALTI). [c] Calculated form 250 m precipitation raster [Joly et al., 2010]. [g] Mean annual Runoff calibrated from figure 4. [h] Catchment discharge variability calculated from thin plane surface fit to the stations estimates (figure 2). [i] Catchment main trunk concavity calculated from 25 m DEM [Perron and Royden, 2012]. [j] Normalized channel steepness index computed using θ_{ref}=0.45. [k] Catchment lithology from 1/10^6 geological map of France (BRGM : Bureau de Recherche Géologique et Minières).

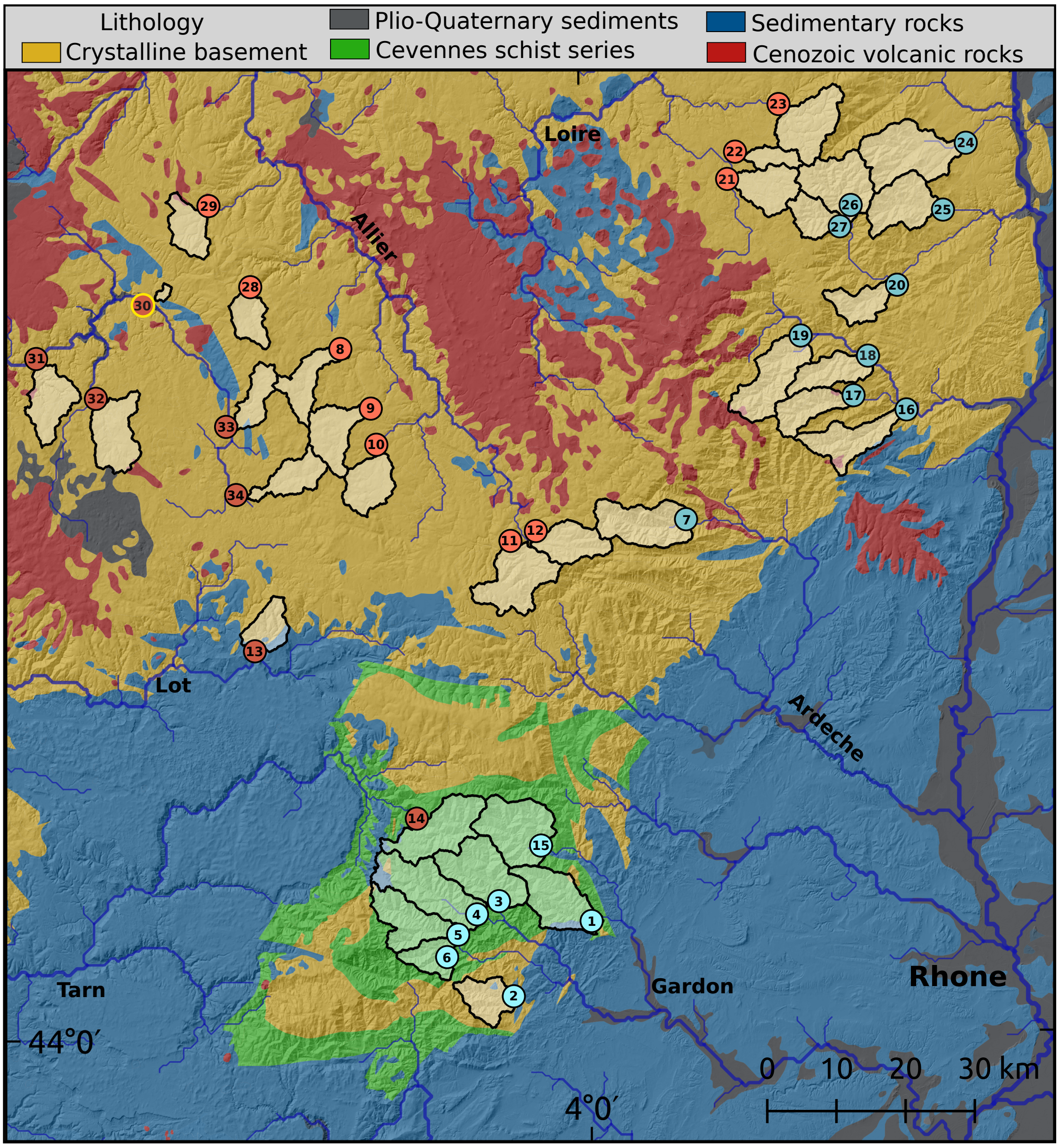

Figure S1: Lithological map of the Southeastern margin of the Massif Central (France), with location of sampled basins. Numbers refer to sample labels.

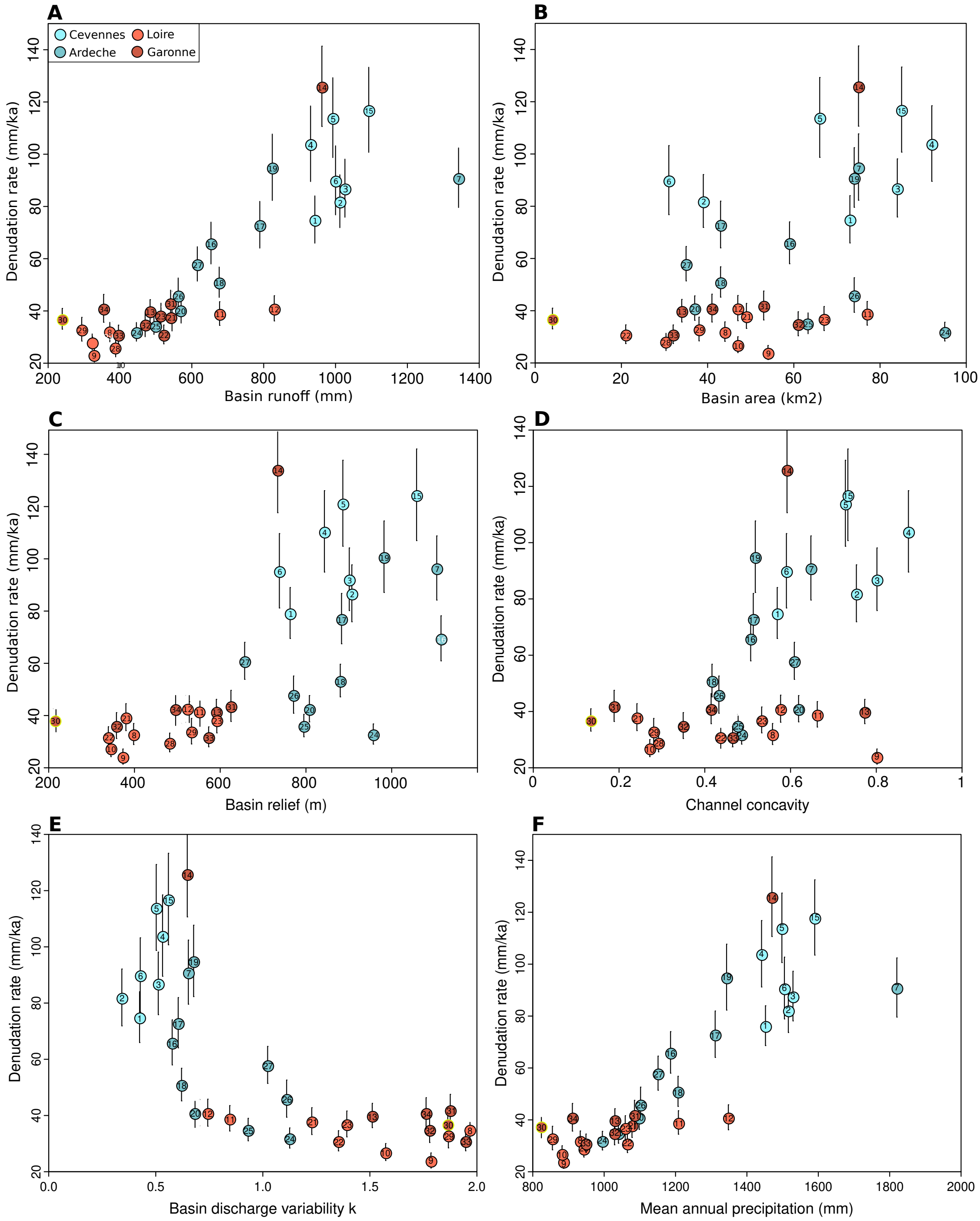

Figure S2: Comparison between denudation rates and various basin parameters (table S3). Symbols are colored according to the location of the catchments (figure 1 and table S3). A - Denudation rate against basin runoff. B - Denudation rate against basin area. C - Denudation rate against basin relief. D - Denudation rate against channel concavity. E - Denudation rate against basin discharge variability. F - Denudation rate against basin mean annual precipitation.

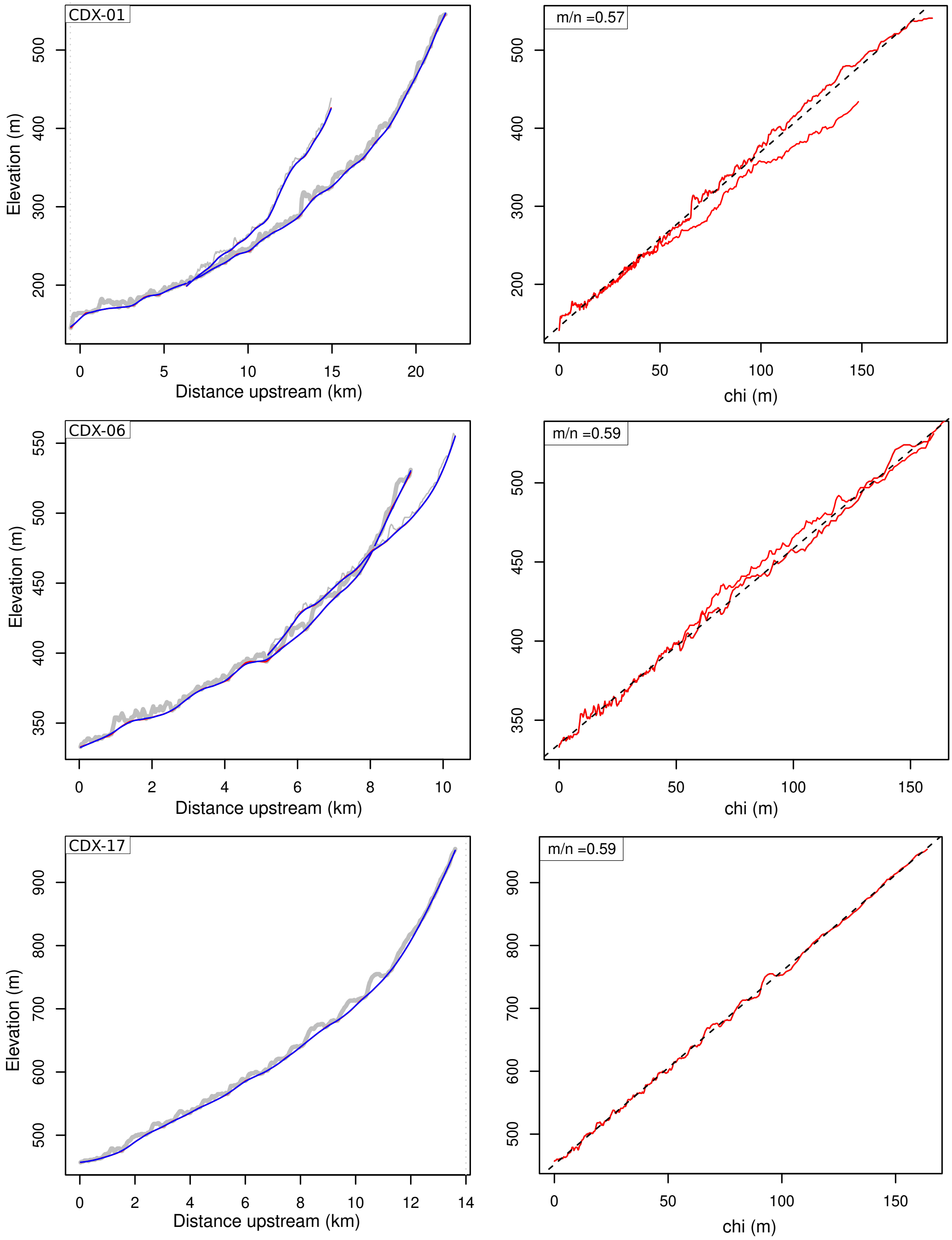

Figure S3: Left panels : longitudinal river profiles for some of the sampled basins in the Cévennes and Ardèche mountains. Grey and blue lines correspond to river profile extracted from IGN BD-ALTI DEM and smoothed river profile with artifacts removed, respectively. Right panels : corresponding Chi-plots for trunk stream optimal concavity determination [Perron and Royden, 2012].

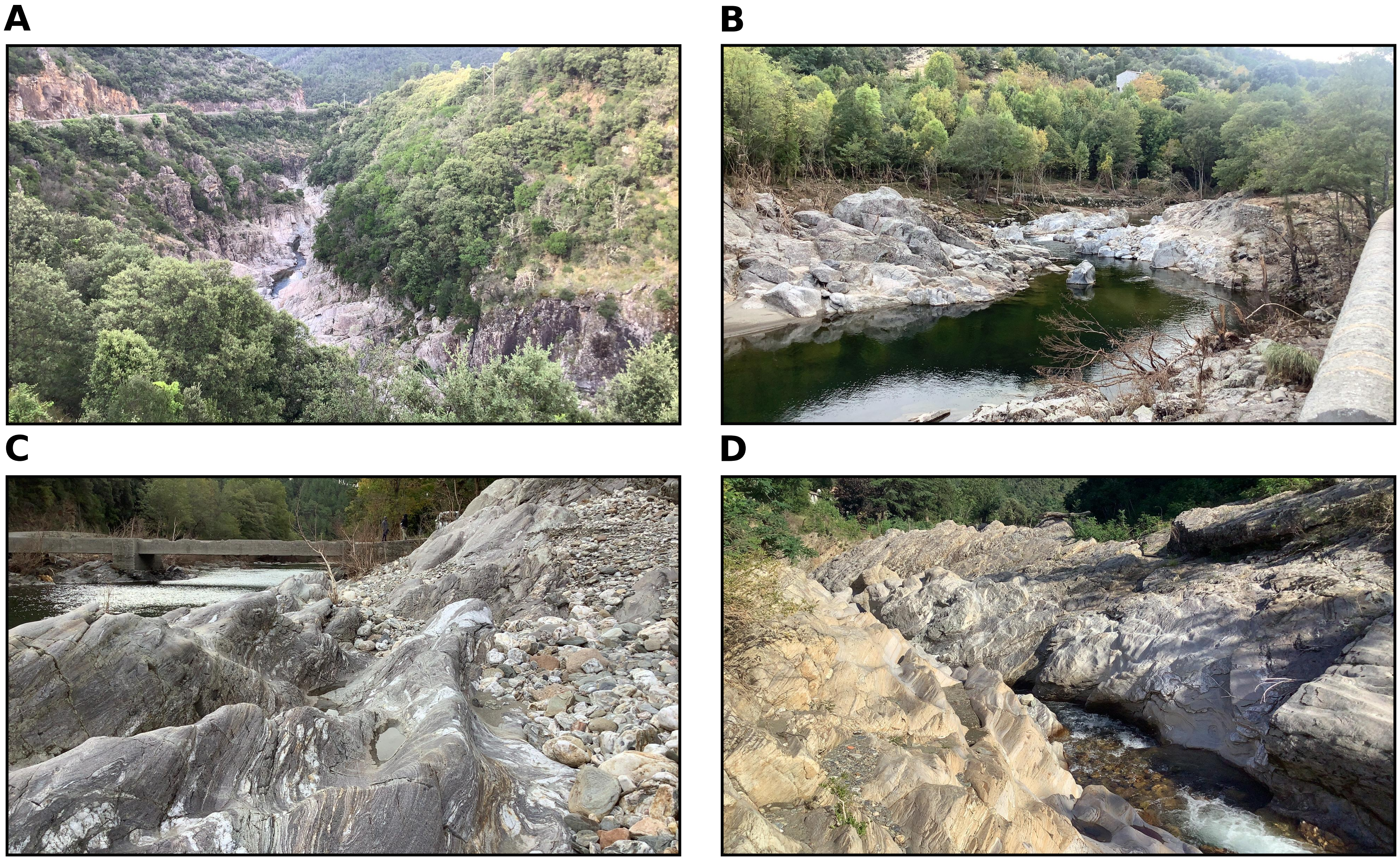

Figure S4: Fields photographs from the Cévennes area. A - Canyon incised into granitic bedrock along the "Gardon de Saint Jean". B - "Gardon de Mialet" river. C - Abrasion figures along the "Gardon de Mialet" river (schist bedrock). D - Incised micashists series along the "Gardon de Saint Jean" river.

References

Arnold, M., Merchel, S., Bourlès, D. L., Braucher, R., Benedetti, L., Finkel, R. C., Aumaître, G., Gottdang, A., and Klein, M. (2010). The French accelerator mass spectrometry facility ASTER: Improved performance and developments. *Nuclear Instruments and Methods in Physics Research, Section B: Beam Interactions with Materials and Atoms*, 268(11-12):1954–1959. ISBN: 0168-583X.

Balco, G. (2017). Production rate calculations for cosmic-ray-muon-produced 10Be and 26Al benchmarked against geological calibration data. *Quaternary Geochronology*, 39:150–173. Publisher: Elsevier B.V.

Balco, G., Stone, J. O., Lifton, N. a., and Dunai, T. J. (2008). A complete and easily accessible means of calculating surface exposure ages or erosion rates from 10Be and 26Al measurements. *Quaternary Geochronology*, 3(3):174–195. ISBN: 1871-1014.

Borchers, B., Marrero, S., Balco, G., Caffee, M., Goehring, B., Lifton, N., Nishiizumi, K., Phillips, F., Schaefer, J., and Stone, J. (2016). Geological calibration of spallation production rates in the CRONUS-Earth project. *Quaternary Geochronology*, 31:188–198. Publisher: Elsevier B.V ISBN: 4025594390.

Braucher, R., Guillou, V., Bourlès, D. L., Arnold, M., Aumaître, G., Keddadouche, K., and Nottoli, E. (2015). Preparation of ASTER in-house 10Be/9Be standard solutions. *Nuclear Instruments and Methods in Physics Research Section B: Beam Interactions with Materials and Atoms*, 361:335–340.

Brown, E. T., Edmond, J. M., Raisbeck, G. M., Yiou, F., Kurz, M. D., and Brook, E. J. (1991). Examination of surface exposure ages of Antarctic moraines using in situ produced 10Be and 26Al. *Geochimica et Cosmochimica Acta*, 55(8):2269–2283. ISBN: 0016-7037.

DiBiase, R. A. (2018). Increasing vertical attenuation length of cosmogenic nuclide production on steep slopes negates topographic shielding corrections for catchment erosion rates. *Earth Surface Dynamics*, 6(4):923–931.

Joly, D., Brossard, T., Cardot, H., Cavailhes, J., Hilal, M., and Wavresky, P. (2010). Types of climates on continental France, a spatial construction. *Cybergeo*, pages 1–25.

Lifton, N., Sato, T., and Dunai, T. J. (2014). Scaling in situ cosmogenic nuclide production rates using analytical approximations to atmospheric cosmic-ray fluxes. *Earth and Planetary Science Letters*, 386:149–160. Publisher: Elsevier B.V.

Merchel, S., Arnold, M., Aumaître, G., Benedetti, L., Bourlès, D., Braucher, R., Alfimov, V., Freeman, S., Steier, P., and Wallner, A. (2008). Towards more precise 10Be and 36Cl data from measurements at the 10-14 level: Influence of sample preparation. *Nuclear Instruments and Methods in Physics Research Section B: Beam Interactions with Materials and Atoms*, 266(22):4921–4926.

Perron, J. T. and Royden, L. (2012). An integral approach to bedrock river profile analysis. *Earth Surface Processes and Landforms*, 38(6):570–576.

von Blanckenburg, F. (2005). The control mechanisms of erosion and weathering at basin scale from cosmogenic nuclides in river sediment. *Earth and Planetary Science Letters*, 237(3-4):462–479.